Zeeman effect and magnetic field induced spin-hybridization in semiconductor quantum dots

2004 J. Phys.: Condens. Matter 16 6949

(http://iopscience.iop.org/0953-8984/16/39/027)

INSTITUTE OF PHYSICS PUBLISHING JOURNAL OF PHYSICS: CONDENSED MATTER

J. Phys.: Condens. Matter **16** (2004) 6949–6960 PII: S0953-8984(04)81221-9

Zeeman effect and magnetic field induced spin-hybridization in semiconductor quantum dots

S J Prado[1], V López-Richard[2], A M Alcalde[1], G E Marques[1] and G Q Hai[2]

[1] Departamento de Física, UFSCar, Caixa Postal 676, 13565-905, São Carlos SP, Brazil
[2] Instituto de Física de São Carlos, USP, 13560-970, São Carlos SP, Brazil

E-mail: vlopez@df.ufscar.br

Received 25 May 2004, in final form 17 August 2004
Published 17 September 2004
Online at stacks.iop.org/JPhysCM/16/6949
doi:10.1088/0953-8984/16/39/027

Abstract

We present a systematic theoretical study of the effective Zeeman spin- and non-linear-splitting of a single spherical quantum dot based on the 8×8 $\mathbf{k} \cdot \mathbf{p}$ Hamiltonian model. The effect of spin-hybridization on conduction band states is pointed out as the main source of the strong dependence of Landè factors and effective masses on external fields. The topology of the electronic orbitals is highly sensitive to the magnetic field tuning and to the spin polarization. The electron, hole and excitonic g-factors, as well as the diamagnetic coefficient are calculated for CdTe semiconductor quantum dots. Different systematic experimental methods are proposed in order to determine the behaviour of the electronic properties under analysis as a function of magnetic field and confinement geometry. Complementary optical transitions, in Faraday and Voigt configurations, can be used in the determination of electron, hole and exciton Landè factors, effective magnetic masses and diamagnetic coefficients.

1. Introduction

A precise knowledge of the effective Landè g-factors is a useful tool for the interpretation of magneto-optical experiments, magneto-transport phenomena, resonant spectroscopy and spin-flip inelastic light scattering. The analysis of Zeeman splitting, related to the Landè factor, and the possible magnetic-tuning mechanisms are important to understand the spin-related effects on the optical response of low-dimensional systems. The topic has attracted increasing interest, from theoretical and experimental points of view [1–6], due to the possibility of spin-engineering in semiconductor nanostructures in the search for applications in spin-polarized magneto-electronics and quantum computation. In recent years, a special emphasis has been

dedicated to the study of mechanisms able to detect and control the spin-polarized states, as important tools for the storage and transmission of information using the spin degrees of freedom. This knowledge requires a constant search for the control of spin coherence throughout practical time and device length scales [7, 8]. Thus, great attention has been focused on the electronic and optical properties of spherical quantum dots (SQDs) [9, 10] as promising systems for the realization of several of these goals.

The combination of spatial and magnetic confinements in nanostructures produces a magnetic-field-dependent dispersion, different from that obtained in bulk semiconductors. Other elements, such as interband coupling and admixture of states, also affect and modify the effective spin-splitting of localized states. This analysis requires an accurate theoretical approach. The study of the main effects that lead to a differentiation of carriers by their spin is the most relevant issue of the present work.

We shall focus special attention on the hybridization of electron spinor states in QDs and shall demonstrate the drastic topological modifications induced by interlevel coupling in that system. We shall describe how these modifications take place and how the induced effects on electronic, magnetic and optical properties can be tuned by external fields. Furthermore, we will discuss how the zinc-blende crystal symmetry may permit a differentiation of the electronic orbitals by their spin orientation. In addition, we propose a systematic experimental framework for unambiguous determination of Landè g-factors and other magnetic properties of carriers. As a complement to the electronic structure calculation, the optical transition selection rules will be derived for the Faraday and Voigt configurations, under different polarizations of the incident light. These complementary configurations are indicated as important tools for the study of optical and magnetic properties. The absorption coefficient has been calculated in order to show that all the reported properties can be submitted to experimental confirmation.

We have developed a systematic calculation of the electronic band structure and band parameters of semiconductor SQDs by using the complete 8×8 $\mathbf{k} \cdot \mathbf{p}$ Kane–Weiler Hamiltonian [11–13] in order to analyse:

(i) the spin-Zeeman splitting induced by the spin-magnetic field interaction, and the determination of the effective Landè factors,

(ii) the linear Zeeman splitting, due to the interaction of the magnetic field and the z-component of the angular momentum, which can provide a direct measure of the excited-state effective masses, and

(iii) the non-linear Zeeman effects associated with the diamagnetic term.

All these effects are found to be highly sensitive to the hybridization of the electronic states. A proper calculation of the electronic structure is important for a detailed analysis of the hybridization tuning of electronic states with different spin orientation. We wish to show that hybridization effects are only reproduced when the band structure calculation is carried out with an adequate mixture of proper symmetries, inherent to the $\mathbf{k} \cdot \mathbf{p}$ Hamiltonian framework, and with the angular orbital coupling to magnetic field being properly taken into account. The qualitative analysis of the spin-hybridization, on the above enumerated effects, can be generalized to any zinc-blende structure. It identifies, both qualitatively and quantitatively, spin-splitting elements that can be attributed directly to different factors such as the effect of quantum confinement, the full Zeeman effect and the angular and spin–orbit coupling. All these factors can be qualitatively described from symmetry properties of the spatial confinement, external fields and lattice structure, which have been all included within the theoretical framework of the 8×8 $\mathbf{k} \cdot \mathbf{p}$ Kane–Weiler model.

2. Spinor states

We shall be working with SQDs of radius R under the weak magnetic field (B_0) regime, $\lambda > R$, where the magnetic scale is defined by the cyclotron length $\lambda = \sqrt{\frac{c\hbar}{eB_0}}$. Thus, we can use a wavefunction expansion on the basis set obtained as the analytical solutions, at $B_0 = 0$, of the diagonal terms (parabolic) in the $\mathbf{k}\cdot\mathbf{p}$ Hamiltonian, for each carrier type: electron (e), heavy-hole (hh), light-hole (lh) and split-off (so). Each eigenstate can be written as an eight-component spinor in the Bloch function space [14], that will be labelled as $|_M\varphi^{N,s}\rangle$. The meaning of each label is: (i) φ, the band index that identifies the carrier type such as $|_M\mathrm{e}^{N,s}\rangle$, $|_M\mathrm{hh}^{N,s}\rangle$, $|_M\mathrm{lh}^{N,s}\rangle$, $|_M\mathrm{so}^{N,s}\rangle$; (ii) $M = -2, -1, 0, 1, 2, \ldots$, an index related to the magnetic number, the only good quantum number of each spinor; (iii) N, the level labelling by increasing energy; (iv) s, the spin polarization of each carrier state [14]. Finally, by studying the symmetry inherent in the $\mathbf{k}\cdot\mathbf{p}$ Hamiltonian we were able to separate the Hilbert space into two orthogonal subspaces [15]. Each component must display a proper parity as determined by the off-diagonal operators in the Hamiltonian. A general spinor state in these subspaces (I and II) has the form

$$|_M\varphi^{N,s}_{\mathrm{I(II)}}\rangle = \sum_{n=1}^{\infty}\sum_{L\geqslant|M|}^{\infty}\begin{pmatrix} f^{M}_{N,2L\ (2L+1)}\,\left|\mathrm{e}^{\uparrow}\right\rangle \\ f^{M-1}_{N,2L+1\,(2L)}\,\left|\mathrm{hh}^{\uparrow}\right\rangle \\ f^{M}_{N,2L+1\,(2L)}\,\left|\mathrm{lh}^{\uparrow}\right\rangle \\ f^{M}_{N,2L+1\,(2L)}\,\left|\mathrm{so}^{\uparrow}\right\rangle \\ f^{M+1}_{N,2L\ (2L+1)}\,\left|\mathrm{e}^{\downarrow}\right\rangle \\ f^{M+2}_{N,2L+1\,(2L)}\,\left|\mathrm{hh}^{\downarrow}\right\rangle \\ f^{M+1}_{N,2L+1\,(2L)}\,\left|\mathrm{lh}^{\downarrow}\right\rangle \\ f^{M+1}_{N,2L+1\,(2L)}\,\left|\mathrm{so}^{\downarrow}\right\rangle \end{pmatrix}, \tag{1}$$

where $f^{M}_{N,L}(r,\Omega) = A^{\varphi}_{N,L}\,\mathbf{j}_L(\alpha_{N,L}r/R)\,Y^{M}_{L}(\Omega)$ and $A^{\varphi}_{N,L}$ is the normalized weight coefficients in the linear combination. Also, $Y^{M}_{L}(\Omega)$ is the spherical harmonic for the solid angle Ω, $\mathbf{j}_L(\alpha_{N,L}r/R)$ is the spherical Bessel function and $\alpha_{N,L}$ is the nth zero of each $\mathbf{j}_L(x)$ function. Finally, $|u^{\uparrow(\downarrow)}\rangle$ represent the four *spin-up* (*spin-down*) periodic Bloch states at the Γ-point of a zinc-blende crystal.

Each Hilbert subspace mixes different spin states with certain spatial geometry, and this mixture will produce significant changes in the carrier energy levels as well as in the topological form of their wavefunctions.

We will use the well known band parameters [15] of CdTe for the calculations, since a considerable amount of recent experimental and theoretical work has focused on the properties of SQDs built on this specific semiconductor [17–20].

3. Hybridization tuning

The degree of state-admixture, within the $\mathbf{k}\cdot\mathbf{p}$ Hamiltonian, will depend on the relative inter- and intra-band energy separation. The nature and strength of interlevel coupling is also determined by their symmetry properties. It should be pointed out that these two factors can be tuned by magnetic field or by an applied axial strain since they induce changes in the spatial symmetry. They can also be treated, within the $\mathbf{k}\cdot\mathbf{p}$ electronic structure calculation, in a natural and general way. In this work we will only focus on the effects associated with the applied magnetic field. We have obtained a strict arrangement of the basis set, for semiconductor SQDs

with zinc-blende symmetry, that combines different spatial distribution probabilities in a very specific way, as shown in equation (1). For a more detailed discussion on the Hamiltonian model and on the basis set see [14–16].

The magnetic field superposes a cylindrical symmetry over the spherical geometry of the SQDs. Under this mixed environment, only the magnetic index, M, remains as a good quantum number in equation (1). We looked for the simplest form to label the *spin-up* and *spin-down* states of each carrier, since they display different values of M, in the Hilbert subspaces I and II. We have chosen to define an effective magnetic number, m^{ef}, determined by the strongest coefficient found at zero magnetic field, in the linear combination which defines the spinor in equation (1). As an example, $m^{\mathrm{ef}} = 0$ labels the pair of *spin-up* and *spin-down* electron states corresponding to $M = -1$ for $|\mathrm{e}^{\downarrow}\rangle$ and $M = 0$ for $|\mathrm{e}^{\uparrow}\rangle$. Notice that the spherical harmonic, $Y_L^{m^{\mathrm{ef}}}(\Omega)$, depends on a particular component in the spinor. This effective magnetic quantum number, m^{ef}, defines the *zero-field slope* of the corresponding linear Zeeman splitting of a given carrier.

The field induces a *magnetic compression* of the states in this mixed geometry and can highlight many interesting hidden properties of SQDs with zinc-blende symmetry, in particular those related to the spin–orbit interaction. Among the effects induced by the interband coupling we will emphasize the hybridization of conduction band spin-split levels and its influence on measurable (observable) electronic properties. This modification of the spin-hybridization will be referred to as *magnetic hybridization tuning*.

In order to understand how this tuning takes place, we will illustrate the process by analysing the behaviour of the largest coefficients in the linear combination, which define the *spin-up* and *spin-down* states in the conduction band, labelled by their effective magnetic quantum number $m^{\mathrm{ef}} = 0$. Since ground-states ($N = 1$) are nearly pure (very small deviation from s-like wavefunction), we are centring our discussion on the first excited states with $N = 2$. After comparing the relative strengths of all components, we can approximate the *spin-up* and *spin-down* state wavefunction as:

$$\left|{}_0\mathrm{e}^{2,\uparrow}\right\rangle \cong \left[A^{\uparrow}_{1,1}\mathbf{j}_1(\alpha_{1,1}r/R)Y_1^0(\Omega)\left|\mathrm{e}^{\uparrow}\right\rangle + A^{\uparrow}_{2,1}\mathbf{j}_1(\alpha_{2,1}r/R)Y_1^1(\Omega)\left|\mathrm{e}^{\downarrow}\right\rangle\right], \tag{2}$$

$$\left|{}_{-1}\mathrm{e}^{2,\downarrow}\right\rangle \cong \left[A^{\downarrow}_{1,1}\mathbf{j}_1(\alpha_{1,1}r/R)Y_1^0(\Omega)\left|\mathrm{e}^{\downarrow}\right\rangle + A^{\downarrow}_{2,1}\mathbf{j}_1(\alpha_{2,1}r/R)Y_1^{-1}(\Omega)\left|\mathrm{e}^{\uparrow}\right\rangle\right]. \tag{3}$$

The factors $A^{\uparrow(\downarrow)}_{1,1}$ and $A^{\uparrow(\downarrow)}_{2,1}$ define the weight of functions with different spatial localization at a given magnetic field and SQD radius. Notice that this approximation is valid for any wide-gap material. Since the well known k-linear Rashba [21] and k-cubic Dresselhauss [22] spin–orbit coupling terms will not be included here, the mixing of conduction band states with different spin polarization, in structures with zinc-blende symmetry, can be obtained only if the coupling with the valence band is included in the calculation, even for wide-gap semiconductors. Electronic states with different spin-orientations and different spatial density distributions 'feel' their mutual presence only by the indirect coupling with holes, as can be seen in the $\mathbf{k}\cdot\mathbf{p}$ model presented in [14–16]. Hence, the simple lack of inversion symmetry of zinc-blende band structures plus the indirect spin–orbit coupling may lead to a complex behaviour of the electronic properties of the spin-split levels in the conduction band.

In figure 1 we show the dependence of weight coefficients on the magnetic field strength for CdTe SQDs with $R = 50$ Å. Near $B_0 = 0$, $A^{\uparrow}_{1,1}$ and $A^{\downarrow}_{1,1}$ are the largest contributions to equations (2) and (3). This will define the magnetic quantum number $m^{\mathrm{ef}} = 0$, for $|{}_0\mathrm{e}^{2\uparrow}\rangle$ and $|{}_{-1}\mathrm{e}^{2\downarrow}\rangle$, since $Y_1^0(\Omega)$ appears as the main component of the angular function, at low fields. This qualitative behaviour can be generalized to any other zinc-blende semiconductor SQDs.

Under *magnetic compression* we observe different reactions of spin-polarized states: the *spin-down* state shows a weaker degree of mixture than the *spin-up* state. This property can be reproduced when the magnetic dispersion of one of the spin-split levels gets closer to a

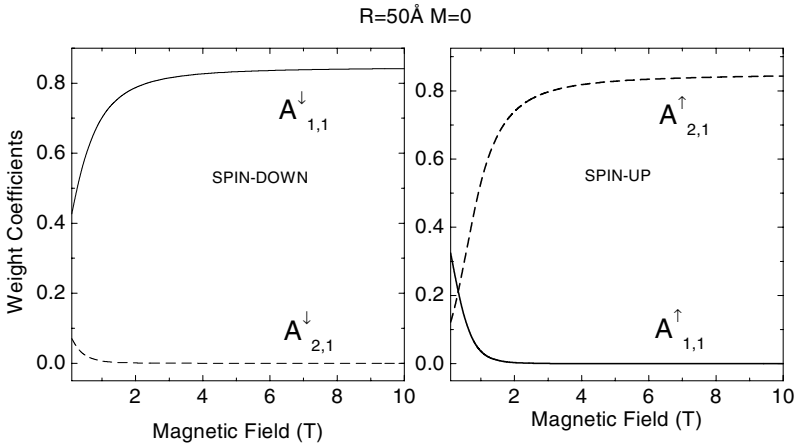

Figure 1. Weight coefficients of the *spin-up* (solid curves) and *spin-down* (dashed curves) states in CdTe SQDs with $m^{\mathrm{ef}} = 0$ and $N = 2$. The largest weights, at zero-field, define the effective magnetic quantum number, m^{ef}.

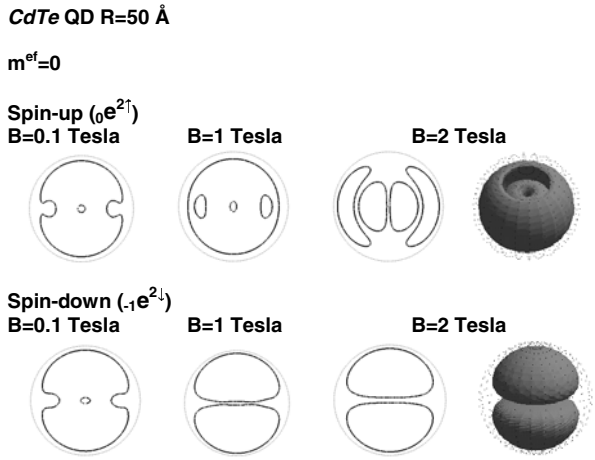

Figure 2. Deformations of the *spin-up* and *spin-down* electronic orbitals, with $m^{\mathrm{ef}} = 0$ and $N = 2$, caused by increasing magnetic compression. The last figure shows the 3D shape at $B_0 = 2$ T.

neighbouring energy-branch. This characteristic can be better visualized by representing the probability density function, according to equations (2) and (3), averaged by the spin. The general modification of the shape of spin-split orbitals, for increasing values of the magnetic field, is shown in figure 2. As the magnetic squeezing increases, the topological structure of the *spin-up*-state orbital undergoes a change from weak sp-like to a d-character, whereas the *spin-down* changes to strong p-like orbital. It is evident that the topology will determine the form and the strength of the carrier interaction with external fields. As will be shown later, these modifications may strongly affect the magnetic properties of spin-split levels and the system optical response. The differentiation of the orbital geometry by the spin orientation may work as an effective tool to control and detect spin-split states.

4. Effective Landè g-factor

Different studies, such as those related to spin-dynamics and quantum computation architecture, depend on the correct interpretation and analysis of g-factors and magneto-optical magnitudes of the corresponding devices [5, 23]. We shall demonstrate how these

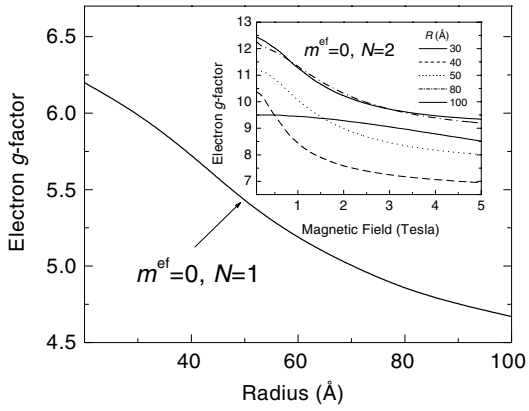

Figure 3. Landè g-factor of the conduction band ground state as a function of the SQD radius at $B_0 = 2$ T. The inset shows the calculated Landè g-factor of conduction band excited states for different dot radii as a function of the magnetic field.

magnitudes are affected by interlevel coupling and by spin-hybridization in zinc-blende SQDs. Furthermore, the non-linear dependence of g-factors on the magnetic field may work as evidence of spin-hybridization processes, if correctly interpreted.

Let us define the effective Zeeman splitting as the difference between the energies $E({}_M\mathrm{e}^{N,\uparrow})$ (*spin-up*) and $E({}_M\mathrm{e}^{N,\downarrow})$ (*spin-down*) of spin-split levels. Thus, the conduction band effective Landè g-factor for the Nth level can be calculated as

$$g_{\mathrm{c}}^{*} = \frac{E\left({}_0\mathrm{e}^{N,\uparrow}\right) - E\left({}_{-1}\mathrm{e}^{N,\downarrow}\right)}{\mu_{\mathrm{B}} B_0}, \tag{4}$$

with $\mu_{\mathrm{B}} = e\hbar/(2m_0c)$ being the Bohr magneton. In figure 3 we show the size dependence of g_{c}^{*}, for the ground state of a CdTe SQD with $m^{\mathrm{ef}} = 0$ and $N = 1$. The inset shows the complex dependence of g_{c}^{*} with magnetic field, for the first excited state with $m^{\mathrm{ef}} = 0$ and $N = 2$. Since the g-factor for the ground state is field-independent, we have not included it within this inset. This is evidence of a very low degree of hybridization for this singlet-type of state. However, for the excited state at $B_0 = 0$, the effect of interlevel mixing enhances the non-parabolicity and induces zero-field splitting. This is the main reason for the anomalous low field dependence of the Landè factor, as shown in the inset of figure 3. It has its origin on the conduction-valence band coupling that is inherent to the $\mathbf{k} \cdot \mathbf{p}$ Hamiltonian, and shows a field dependence that is identical to the anomalous Zeeman and Paschen-Back regimes found in atoms [24].

At relatively high magnetic fields, the strength of interlevel mixing fades off and the g-factors become pinned to almost constant values. In other words, the interlevel separation is enhanced by the magnetic confinement which, in turn, increases the absolute value of the g-factor [15, 25, 26]. For larger dot sizes, g_{c}^{*} should become pinned to the bulk values, which our theory cannot reproduce since we are restricted to the regime $\lambda > R$.

The magnetic tuning of the Zeeman splitting can be used as a measure of the level admixture, since the deviations from the single-band model should be unambiguously attributed to the interband mixing. An intense search for the tuning of g-factors [27] is in course because of its possible application in quantum-information transmission devices. It is important to notice that an energy crossing of the spin-split levels can take place at certain SQD radius, leading to a sign inversion of Landè factors for excited states. The conditions for the sign inversion depend on band parameters and may vary from one material to another. However, it is an effect that can be observed in different materials and for different shapes of spatial confinements where, once more, the differentiation of spin-split levels plays an important role. The necessary turnover of a level dispersion with the magnetic field, that ultimately

Table 1. Selection rules for the strongest transitions using the magnetic number m^{ef}.

Electric dipole transitions in SQDs					
σ^+		σ^-		Π^z	
$\mathrm{hh}\uparrow \to \mathrm{e}\uparrow$	$\Delta m^{\mathrm{ef}} = 2$	$\mathrm{hh}\downarrow \to \mathrm{e}\downarrow$	$\Delta m^{\mathrm{ef}} = -2$	$\mathrm{lh}\downarrow \to \mathrm{e}\uparrow$	$\Delta m^{\mathrm{ef}} = -1$
$\mathrm{hh}\downarrow \to \mathrm{e}\downarrow$	$\Delta m^{\mathrm{ef}} = 0$	$\mathrm{hh}\uparrow \to \mathrm{e}\uparrow$	$\Delta m^{\mathrm{ef}} = 0$	$\mathrm{lh}\downarrow \to \mathrm{e}\downarrow$	$\Delta m^{\mathrm{ef}} = 0$
$\mathrm{lh}\downarrow \to \mathrm{e}\uparrow$	$\Delta m^{\mathrm{ef}} = 0$	$\mathrm{lh}\uparrow \to \mathrm{e}\downarrow$	$\Delta m^{\mathrm{ef}} = 0$	$\mathrm{lh}\uparrow \to \mathrm{e}\uparrow$	$\Delta m^{\mathrm{ef}} = 0$
$\mathrm{lh}\downarrow \to \mathrm{e}\downarrow$	$\Delta m^{\mathrm{ef}} = 1$	$\mathrm{lh}\uparrow \to \mathrm{e}\uparrow$	$\Delta m^{\mathrm{ef}} = -1$	$\mathrm{lh}\uparrow \to \mathrm{e}\downarrow$	$\Delta m^{\mathrm{ef}} = 1$

determines the position of the spin-split level crossing, is determined by the coupling between neighbouring states.

The process of spin differentiation would be of little interest if it were difficult to measure. We are showing below that optical interband transitions, using complementary configurations, provide a clear tool to study the effective Zeeman splitting of electrons and holes, despite their complex dependence on external fields. Let us assume an incident light along the magnetic field direction, taken as the z axis. We shall consider two major configurations: (i) the incident light with circular polarization $\hat{\mathbf{e}} = \left(\hat{\mathbf{e}}_x \pm \mathrm{i}\hat{\mathbf{e}}_y\right)/\sqrt{2}$, in Faraday configuration, denoted as $\sigma^{\pm}$; (ii) the incident light with linear polarization $\hat{\mathbf{e}} = \hat{\mathbf{e}}_z$, in Voigt configuration, denoted as Π^z. After calculating the interband selection rules for SQDs we have observed that certain transitions show a relatively strong strength (see [15]) and some of them are listed in table 1.

We can use the absorption resonant-peak energies to obtain information on the relative position of conduction band levels. When two different interband transitions have the same initial valence band level, then the distance between the corresponding resonances equals the separation between the final conduction band levels involved. By observing table 1, this condition can be accomplished by using linear (Π^z) and circular polarizations ($\sigma^{\pm}$) in Voigt and Faraday configurations, respectively; this determines both the conduction band Zeeman splitting and the corresponding Landè factor [15], as

$$g_{\mathrm{c}}^{*}\,\mu_{\mathrm{B}}\,B_0 = \Delta E^{\Pi^z}\left({}_{M}\mathrm{lh}^{N,\uparrow} \to {}_{M}\mathrm{e}^{N,\uparrow}\right) - \Delta E^{\sigma^-}({}_{M}\mathrm{lh}^{N,\uparrow} \to {}_{M+1}\mathrm{e}^{N,\downarrow}), \qquad (5)$$

where $\Delta E^{\eta}(\alpha \to \alpha')$ denotes the interband energy of an electron (α')–hole (α) pair, obtained in a given configuration (η) of the incident light. In figure 4(a) we show the complementary magneto-absorption spectra for Π^z and σ^+ configurations, calculated for a SQD with radius $R = 30$ Å, at different values of magnetic field. As seen in table 1, the indicated transitions have the same initial valence state. Therefore, the energy separation between the resonant peaks yields the conduction band Zeeman splitting. The conduction band g-factor (shown in figure 3) can be directly extracted from these optical absorption measurements, using equation (5).

By analogous reasoning we can also obtain the excitonic g-factor, g_{ex}^{*}, that includes both electron and hole contributions, determined by other two complementary polarizations. Since the effects of spatial confinement is much stronger than the electron–hole pair Coulomb interaction within the regime $\lambda > R$, we can describe excitons here as nearly uncoupled electron–hole pairs. Thus, excitonic Landè factors can be determined by combining the spectra of opposite circular polarizations, σ^+ and σ^- in Faraday configuration (see table 1) as

$$g_{\mathrm{ex}}^{*}\,\mu_{\mathrm{B}}\,B_0 = \Delta E^{\sigma^-}({}_{M}\mathrm{hh}^{N,\uparrow} \to {}_{M-1}\mathrm{e}^{N,\uparrow}) - \Delta E^{\sigma^+}({}_{M-3}\mathrm{hh}^{N,\downarrow} \to {}_{M-2}\mathrm{e}^{N,\downarrow}). \qquad (6)$$

In figure 4(b) we show the complementary optical transitions involved in the determination of the excitonic g-factor, for the same dot of figure 4(a), using two opposite circular polarizations. These spectra show that the relevant absorption lines, in the complementary configurations, permit the obtention of the effective excitonic Zeeman splitting. The dot size dependence of the excitonic g-factor, calculated from equation (6) and using the complementary absorption

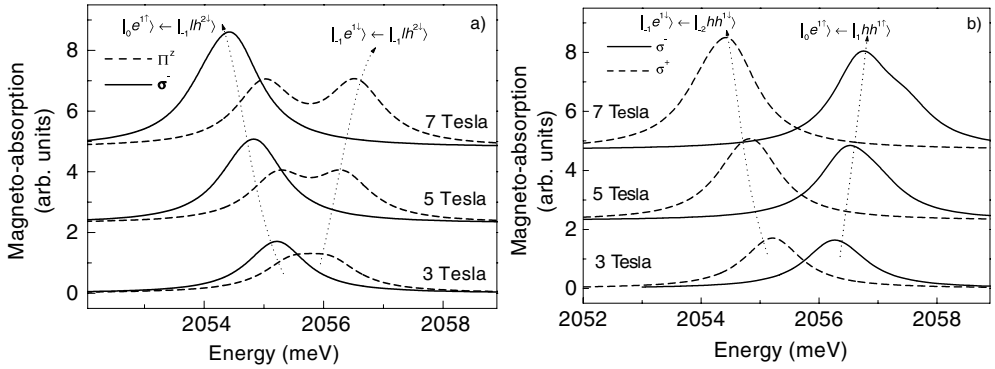

Figure 4. Calculated magneto-absorption spectra in σ^+ and Π^z, Farady and Voigt configurations, respectively, at various magnetic fields. The relative distance between resonant peaks of complementary polarizations defines the conduction band Zeeman splitting. (b) Magneto-absorption spectra in σ^+ and σ^- Faraday configurations, for various magnetic fields. The relative distance between resonant peaks corresponds to the effective excitonic Zeeman splitting. The diagrammatic representation of the involved transitions in both complementary configurations are also shown.

spectra of figure 4(b), is shown in figure 5. As can be seen, the excitonic Zeeman splitting is strongly dependent on the dot size and combines the effects of both electron and hole spin-splitting. Furthermore, since the electron spin-splitting can be determined independently, we can also obtain the values of valence band g-factors, by knowing the corresponding values of $g^*_{\rm ex}$ and $g^*_{\rm c}$.

By using the definition of the g-factor in excitonic complexes as

$$g^{\rm hh*}_{\rm ex} = g^*_{\rm c} + 3 \cdot g^*_{\rm hh}, \tag{7}$$

$$g^{\rm lh*}_{\rm ex} = g^*_{\rm c} + g^*_{\rm lh}, \tag{8}$$

we can easily calculate the valence band Landè factors for heavy ($g^*_{\rm hh}$) or light ($g^*_{\rm lh}$) holes. The numeric factor 3 (1) multiplying $g^*_{\rm hh}$ ($g^*_{\rm lh}$) has its origin in the total spin $\frac{3}{2}$ ($\frac{1}{2}$) of heavy-(light-) hole Bloch state at the Γ-point. The g-factors of heavy (solid curve) and light (dashed curve) holes in CdTe SQDs, calculated as a function of the dot radius, are shown in the inset of figure 5. Once again they are sensitive to the size of the confining region. The valence band g-factor dependence on size, obtained from the excitonic spin-splitting, has usually been neglected [8], however it proves to be important. Within the dot-radius range, considered in the calculation shown in figure 5, the valence band contribution consists of almost 20% of the combined electron–hole pair spin-splitting effect.

Finally, if the energy separation between two spin-split magnetic branches in the valence band becomes very small, their enhanced degree of mixture may induce a sign-change in the g-factors whenever the dispersion of states ${}_M{\rm hh}^{N,\uparrow}$ and ${}_{M-3}{\rm hh}^{N,\downarrow}$ displays a crossing region. This actually happens at some critical values of $B_0 = B_{\rm c}$ for a specific spatial confinement. The critical values of the magnetic field, where the sign inversion takes place, depend also on the specific material and band parameters.

5. Anomalies in the linear Zeeman effect and diamagnetic shift

The spin-hybridization affects the behaviour of the linear Zeeman effect and also modulates the non-linear contributions associated with the diamagnetic term. Both effects can be of great importance to determine the effective masses as well as orbital topology. These anomalies

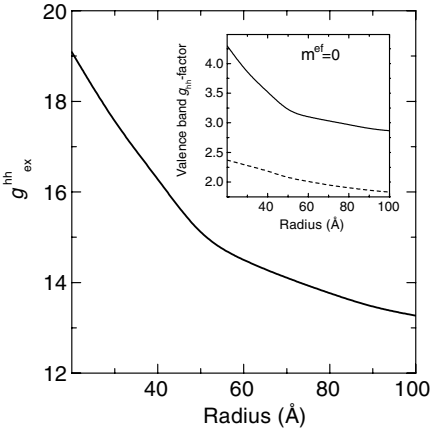

Figure 5. Calculated excitonic g-factor from complementary magneto-absorption spectra as a function of the SQD radius at $B_0 = 2$ T. The inset shows the calculated valence band g-factor of heavy-hole (solid curve) and light-hole (dashed curve) as a function of the dot radius using σ^+ and Π^z complementary magneto-absorption configurations.

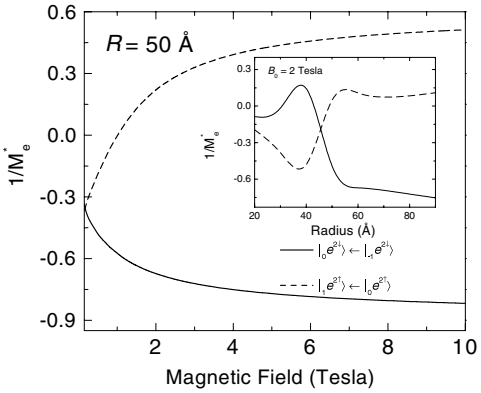

Figure 6. Calculated electron magnetic-effective mass from the linear Zeeman splitting as a function of the dot size and the magnetic field strength.

are directly related to magnetic quantization of states and, within the non-parabolic multiband effective mass approximation, they are strongly spin-dependent.

The linear Zeeman effect for each carrier can be attributed to the state-quantization induced by the coupling between the angular momentum and the external magnetic field, $H = (\hbar e/cM^*)g^*L_zB_0$. Let us focus on the states in the conduction band. For spherical confinements this coupling generates a fan of magnetic levels with slopes depending on the effective magnetic quantum number, $m^{\rm ef}$, and is proportional to $1/M^*_e$. Having found the magnetic numbers, $m^{\rm ef}$, we can determine the electron magnetic-effective mass from the slope of the corresponding level dispersion, for each spin-polarization. In the present case, the magnetic-mass can be calculated as

$$\frac{1}{M^*_{{\rm e}\uparrow(\downarrow)}} = \left(\frac{2c}{\hbar e}\right)\frac{E(_{M+1}{\rm e}^{N\uparrow(\downarrow)}) - E(_{M}{\rm e}^{N\uparrow(\downarrow)})}{B_0}. \tag{9}$$

The dependence of $1/M^*_{{\rm e}\uparrow(\downarrow)}$ with magnetic field, as shown in figure 6, exhibits a singular behaviour at relatively low values of B_0. The coupling between states with different (equal) values of magnetic numbers M ($m^{\rm ef}$) is inversely proportional to their interlevel energy separation. This coupling may eventually lead to the crossing between M and $M+1$ energy branches shown in equation (9). The behaviour of effective masses may show a stronger anomaly when analysed as a function of the dot radius R since the strength of the spatial confinement induces changes in the relative positions of the spin-split levels. Observe, in equation (9), that an inversion of the sign in the magnetic mass of spin-split states, as shown in figure 6, can be associated with an interchange between the relative energy level positions.

At higher fields we observe a large magnetic-mass difference between *spin-up* and *spin-down* states. As already discussed in figure 2, the spatial distribution-densities of these states change between different topologies as the magnetic field increases. Therefore, the axial magnetic squeezing originates in the anomaly of the effective masses shown in figure 6.

The optical selection rules, as shown in table 1, ensure a direct determination of the linear Zeeman splitting and the magnetic effective masses from optical measurements, by using the

same set of complementary $\sigma^{+(-)}$ and Π^z configurations used to determine the electron g-factor. It is important to observe another anomaly, for CdTe dot sizes between 40–60 Å, where the inverse magnetic effective masses display an interchange of values. In this particular region near $R = 50$ Å an interchange of character takes place between the conduction band electron states produced by the strong state admixture [15]. The spin-hybridization has led to this particular behaviour in the magnetic properties associated with the linear Zeeman contribution. The response to a magnetic field strongly depends on the effective mass, thus the reported effect can be used so as to unambiguously differentiate carriers by their spin orientation.

Finally, small contributions derived from higher order magnetic terms have been attributed to diamagnetic corrections [28–30], which can be relevant for the qualitative analysis of topological modifications to the charge-density distribution. Anomalous magnetic effects are also induced by the diamagnetic Hamiltonian that has a general form $(H_D, \tilde{}\rho B_0^2)$. The induced diamagnetic shift can be calculated from the excitonic transition energies, $\Delta E^{\sigma+(-)}[{}_M\mathrm{hh}^{N,\downarrow(\uparrow)} \rightarrow_{M+1(M-1)} \mathrm{e}^{N,\downarrow(\uparrow)}]$, where the diamagnetic coefficient ρ, is a function of B_0 and measures an average square localization, $\langle r^2 \rangle$, of carriers in the mixed axial plus spherical confinement geometries. For each light polarization, the excitonic diamagnetic coefficient can be calculated as

$$\rho\left(\sigma^{+(-)}, B_0\right) = \frac{1}{2}\frac{\partial^2 \Delta E^{\sigma+(-)}[{}_M\mathrm{hh}^{N,\downarrow(\uparrow)} \rightarrow_{M+1(M-1)} \mathrm{e}^{N,\downarrow(\uparrow)}]}{\partial B_0^2}. \tag{10}$$

Since $\rho\left(\sigma^{+(-)}, B_0\right)$ is a measure of the average localization, it can be a signature of the orbital topologies shown in figure 2. We can thus analyse how it is affected by the competition between magnetic field strength and dot size. The diamagnetic shift has been calculated here in order to evaluate the magnitude of the induced magnetic deviations for the lowest conduction band levels of a CdTe SQD. The dependence of $\rho\left(\sigma^{+(-)}, B_0\right)$ on magnetic field is shown in figure 7 for different dot sizes. Depending on the polarization of the incident light, one can populate a specific spin-polarized ground state. The spin orientation defines two quantitatively and qualitatively different responses. This is clear evidence of a hidden non-parabolicity induced by interband magnetic coupling within the $\mathbf{k} \cdot \mathbf{p}$ method. Moreover, the different dependence of $\Delta E^{\sigma+(-)}$ on field strength, for the same dot size, are directly related to different orbital topologies of spin-polarized states in SQDs, as discussed in figure 2.

The *spin-up* state, populated during the σ^- optical excitation (see figure 7(a)), exhibits a much stronger magnetic compression than the *spin-down* state, populated with σ^+ incident light polarization (see figure 7(b)). At large enough dot-radii, $\rho\left(\sigma^-, B_0\right)$ displays a nearly parabolic dependence on B_0 for the *spin-up* state, whereas, for the corresponding *spin-down* state, $\rho\,(\sigma^+, B_0)$ shows a linear dependence. This difference implies that the effective confinement of the *spin-up* state is one order of magnitude more sensitive to the magnetic compression than the *spin-down* state. It also confirms our prior discussion on the topological differences between the spin-split levels. Another interesting fact, even for the 'mutant' *spin-up* state, is the existence of a threshold where the effects due to magnetic confinement become negligible. For sufficiently small dot sizes, the *spin-up* state shows almost no magnetic squeezing, indicating that the spatial confinement dominates over any other localization effect.

Recent available experimental results have confirmed these strong influences of QD size and magnetic field on the diamagnetic coefficient ρ [31, 32]. The diamagnetic energy-shift has also been measured for CdSe/ZnSe QDs, using Faraday geometry, and a strong red-shift has been reported for dot radii near 50 Å. An interesting feature, to be pointed out here, is the rather different dependence on B_0, as shown in figure 7, between the calculated diamagnetic coefficients in Faraday geometry with σ^+ and σ^- polarizations. An analogous behaviour has been experimentally observed by Sugisaki *et al* in self-assembled InP QDs [32], where the

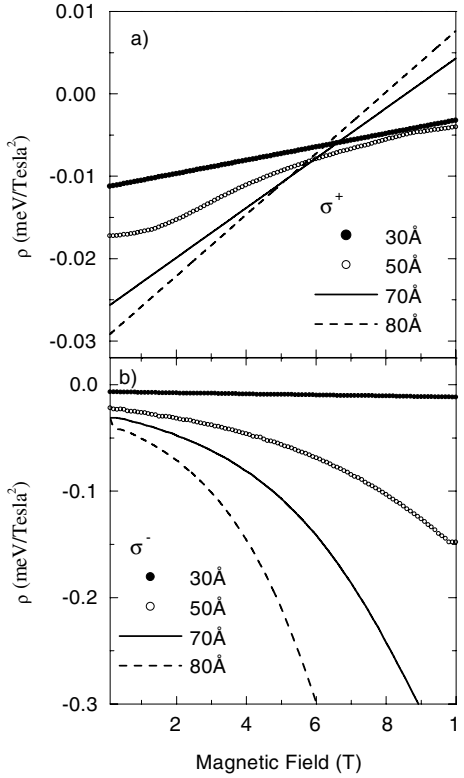

Figure 7. Calculated diamagnetic localization length scale for spin-polarized ground states as a function of the magnetic field and dot radius. (a) Light excitation with σ^+ polarization populates the *spin-up* state. (b) Light excitation with σ^- polarization populates the *spin-down* state.

shift in the PL peak for σ^+-polarization is larger than those measured with σ^--polarization. It has also been reported that the diamagnetic coefficient decreases gradually with the growth of QD size, which confirms our theoretical predictions.

6. Conclusions

In summary, we were able to study the consequences of a dimensionality reduction on different contributions to the Zeeman effect in SQDs within the framework of the $\mathbf{k} \cdot \mathbf{p}$ multiband effective-mass approximation. We have shown that the interband coupling can induce a strong spin-hybridization of the carrier magnetic-dispersions. The mixing of states with different spin may drastically modify the topology of the spatial density of carriers. The competition between the magnetic compression and spatial confinement leads to anomalous behaviours of the effective Landè factors, magnetic effective masses, and diamagnetic shifts on B_0. An optical experimental method has been proposed in order to verify and explore the effects theoretically revealed here. We have demonstrated that the effective g-factors and effective masses, for the ground and excited states, can be experimentally obtained from complementary magneto-absorption configurations. The calculated g-factors for excited states have shown a complex field dependence that can be interpreted as a measure of spin-hybridization in the conduction band. The calculated effective masses and diamagnetic corrections have enlightened some effects that can be used for the differentiation of carrier behaviour in terms of their spin orientation. These effects are all induced by the proper introduction of the spin–orbit interaction within the electronic structure calculation.

We would like to point out that the physics of spin-polarized states, related to the search for spintronic devices, and the success of studies addressing the spin dynamics for quantum computation architecture, depend on an accurate determination of the Landè g-factor and its dependence on external fields and spatial confinement. We should also remark that the spin-hybridization due to spin–orbit coupling and inter-band admixture are mutually correlated characteristics, inherent to each system. Thus, any attempts to reduce these effects into a combination of single components is clearly impossible. We hope that this analysis will provide new insights into magnetic and electronic properties in semiconductor nanostructures, enlightening the discussions of spin-related phenomena in zinc-blend type SQDs.

Acknowledgments

This work has been supported by Fundação de Amparo à Pesquisa do Estado de Sâo Paulo (FAPESP) and by Conselho Nacional de Desenvolvimento Científico e Tecnológico (CNPq), Brazil. Also we are in debt to C Trallero-Giner for long discussions on this subject.

References

[1] Sirenko A A, Ruf T, Cardona M, Yakovlev D R, Ossau W, Waag A and Landwehr G 1997 *Phys. Rev.* B **56** 2114
[2] Sirenko A A, Belitsky V I, Ruf T, Cardona M, Ekimov A I and Trallero-Giner C 1998 *Phys. Rev.* B **58** 2077
[3] Kotlyar R, Reinecke T L, Bayer M and Forchel A 2001 *Phys. Rev.* B **63** 085310
[4] Medeiros-Ribeiro G, Pinheiro M V B, Pimentel V L and Marega E 2002 *Appl. Phys. Lett.* **80** 4229
[5] Kiselev A A, Ivchenko E L and Rössler U 1998 *Phys. Rev.* B **58** 16353
[6] Chang K, Xia J B and Peeters F M 2003 *Appl. Phys. Lett.* **82** 2661
[7] Gupta J A, Awschalom D D, Peng X and Alivisatos A P 1999 *Phys. Rev.* B **59** 10421
[8] Gupta J A, Awschalom D D, Efros Al L and Rodina A V 2002 *Phys. Rev.* B **66** 125307
[9] Masumoto Y and Ogasawara S 2000 *J. Lumin.* **87–89** 360
[10] Woggon U 1997 *Optical Properties of Semiconductor Quantum Dots* (Berlin: Springer)
[11] Kane E O 1957 *J. Phys. Chem. Solids* **1** 249
[12] Weiler M H 1966 *Magnetooptical Properties of* $Hg_{1-x}Cd_xTe/CdTe$ *Alloys, Semiconductors and Semimetals* vol 16, ed R K Willardson and A C Beer (New York: Academic)
[13] López-Richard V, Marques G E and Trallero-Giner C 2000 *Solid State Commun.* **114** 649
López-Richard V, Marques G E and Trallero-Giner C 2000 *Solid State Commun.* **115** 515
[14] Prado S J, Trallero-Giner C, Alcalde A M, López-Richard V and Marques G E 2003 *Phys. Rev.* B **68** 235327
[15] Prado S J, Trallero-Giner C, Alcalde A M, López-Richard V and Marques G E 2003 *Phys. Rev.* B **67** 165306
[16] Prado S J, Trallero-Giner C, Alcalde A M, López-Richard V and Marques G E 2004 *Phys. Rev.* B **69** R201310
[17] Efros A L and Rosen M 1998 *Phys. Rev.* B **58** 7120
[18] Besombes L, Kheng K, Marsal L and Marlette H 2002 *Phys. Rev.* B **65** 121314
[19] Lavattard P, Petrikov V D and Lipovskii A A 2001 *Phys. Rev.* B **64** 113303
[20] Shen M Y, Oda M and Goto T 1999 *Phys. Rev. Lett.* **82** 3915
[21] Voskoboynikov O, Lee C P and Tretyak O 2001 *Phys. Rev.* B **63** 165306
[22] Dresselhaus G 1955 *Phys. Rev.* **100** 580
[23] Nomura S, Segawa Y and Kobayashi T 1994 *Phys. Rev.* B **49** 13571
[24] See for example, Sakurai J J 1994 *Modern Quantum Mechanics* (Reading, MA: Addison-Wesley)
[25] Thornton A S G, Ihn T, Main P C, Eaves L and Henini M 1998 *Appl. Phys. Lett.* **73** 354
[26] Kuno M, Nirmal M, Bawendi G, Efros A and Rosen M 1998 *J. Phys. Chem.* **108** 4242
[27] Chang K, Xia J B and Peeters F M 2003 *Appl. Phys. Lett.* **82** 2661
[28] Planelles J, Díaz J G, Climente J and Jaskólski N 2002 *Phys. Rev.* B **65** 245302
[29] Wang P D, Merz J L, Fafard S, Leon R, Medeiros-Ribeiro G, Oestreich M, Petroff P M, Uchida K, Miura N, Akiyama H and Sakaki N 1996 *Phys. Rev.* B **53** 16458
[30] Bayer M, Walck S N, Reinecke T L and Forchel A 1958 *Phys. Rev.* B **57** 6584
[31] Miura N K, Yasuhira T, Kurtz E, Klingshirn C, Nakashima H, Issiki F and Shiraki Y 2002 *Physica* E **13** 263
[32] Sugisaki M, Ren H, Nair S V, Nishi K and Masumoto Y 2002 *Phys. Rev.* B **66** 235309